Subunit III of Cytochrome *c* Oxidase of *Rhodobacter sphaeroides* Is Required To Maintain Rapid Proton Uptake through the D Pathway at Physiologic pH[†]

Gwen Gilderson,[‡] Lina Salomonsson,[‡] Anna Aagaard,[‡] Jimmy Gray,[§] Peter Brzezinski,[‡] and Jonathan Hosler*[,§]

Department of Biochemistry and Biophysics, The Arrhenius Laboratories for Natural Sciences, Stockholm University, SE-106 91 Stockholm, Sweden, and Department of Biochemistry, University of Mississippi Medical Center, 2500 North State Street, Jackson, Mississippi 39216

Received January 22, 2003; Revised Manuscript Received April 22, 2003

ABSTRACT: The catalytic core of cytochrome *c* oxidase is composed of three subunits where subunits I and II contain all of the redox-active metal centers and subunit III is a seven transmembrane helix protein that binds to subunit I. The N-terminal region of subunit III is adjacent to D132 of subunit I, the initial proton acceptor of the D pathway that transfers protons from the protein surface to the buried active site ∼30 Å distant. The absence of subunit III only slightly alters the initial steady-state activity of the oxidase at pH 6.5, but activity declines sharply with increasing pH, yielding an apparent pK_a of 7.2 for steady-state O_2 reduction. When subunit III is present, cytochrome oxidase is more active at higher pH, and the apparent pK_a of steady-state O_2 reduction is 8.5. Single-turnover experiments show that proton uptake through the D pathway at pH 8 slows from >10000 s^{-1} in the presence of subunit III to 350 s^{-1} in its absence. At low pH (5.5) the D pathway of the oxidase lacking subunit III regains its capacity for rapid proton uptake. Analysis of the **F** → **O** transition indicates that the apparent pK_a of the D pathway in the absence of subunit III is 6.8, similar to that of steady-state O_2 reduction (7.2). The pK_a of D132 itself may decline in the absence of subunit III since its carboxylate group will be more exposed to solvent water. Alternatively, part of a proton antenna for the D pathway may be lost upon removal of subunit III. It is proposed that one role of subunit III in the normal oxidase is to maintain rapid proton uptake through the D pathway at physiologic pH.

As the terminal member of the respiratory electron-transfer chain in mitochondria and many aerobic bacteria, the aa_3-type cytochrome *c* oxidase reduces oxygen to water and uses some of the energy of the electron-transfer process to pump four protons through the protein, across the membrane, for each O_2 reduced. The three largest subunits, I, II, and III, form the catalytic core of the enzyme. Electrons from cytochrome *c* are first transferred to the dicopper Cu_A center in subunit II. Electrons from Cu_A flow to the six-coordinate heme *a* in subunit I and then onto the heme a_3−Cu_B site in subunit I, where O_2 is reduced. During catalysis, the protons required for the reduction of oxygen, as well as those that are pumped through the protein, are taken up from the inner surface of the protein (facing the mitochondrial matrix or bacterial cytoplasm). The protons are transferred through two specific pathways to the buried heme a_3−Cu_B active site some 30 Å into the transmembrane region of the protein (*1*). The K pathway (named for a conserved lysine of the pathway) is responsible for the uptake of one or two protons during the "reductive" phase of the catalytic cycle, when heme a_3 and Cu_B are being reduced prior to the binding of O_2 (*2*−*4*). The D pathway, named for a conserved aspartic acid residue that serves as the initial proton acceptor of the pathway, transfers the remaining "substrate" protons to the active site for O_2 reduction plus all of the pumped protons (*5*−*7*). The D pathway is composed of different regions (*8*−*10*). The first is a pathway that connects D132, the initial acceptor, with E286, located ∼26 Å above D132. A series of highly ordered water molecules, plus an asparagine residue (N139), forms a hydrogen-bonded proton-conductive pathway between these two carboxylates. A second series of waters extends from E286 to the heme a_3−Cu_B center, a distance of 10−12 Å (*11*). These waters may be oriented in several conformers since they are not resolved in the crystal structure (*10*). The maximum rate of proton transfer through both of these hydrogen-bonded proton-conductive paths of the D pathway is rapid, at least 10000 s^{-1} (*12*, *13*). Finally, protons presumably flow from E286 to the site of proton pumping, located at or near the active site (*14*−*16*).

Much of the chemistry of O_2 reduction by cytochrome oxidase has been elucidated through optical and resonance Raman analyses of the reduction of a single O_2 by the fully reduced oxidase (*17*−*20*). In the flow−flash technique (*21*) carbon monoxide (CO) is bound to fully reduced cytochrome oxidase, the CO-bound oxidase is mixed with oxygenated buffer, and the reduction of O_2 is simultaneously initiated in the entire population of oxidase molecules by a laser flash that releases the bound CO and allows O_2 to bind. Reduction of the bound O_2 rapidly produces the $\mathbf{P_R}$ intermediate, which

[†] Supported by National Institutes of Health Grant GM56824 (to J.H.) and The Swedish Research Council, The Swedish Foundation for International Co-operation in Research and Higher Education, and the Human Frontier Science Program (to P.B.).

* Corresponding author. Telephone: 601-984-1861. Fax: 601-984-1861. E-mail: jhosler@biochem.umsmed.edu.

[‡] Stockholm University.

[§] University of Mississippi Medical Center.

10.1021/bi0341298 CCC: $25.00
Published on Web 05/29/2003

consists of an oxyferryl on heme a_3 (a_3^{4+}=O) and a hydroxyl group on Cu_B (Cu_B-OH^-) (*18*, *22*−*24*). Following this, the **F** intermediate is formed by the transfer of a proton through the D pathway to the hydroxyl group on Cu_B, forming one water (*12*, *25*). The final step is the conversion of **F** to **O** (oxidized), a step which requires the simultaneous reduction and protonation of the heme a_3 oxyferryl, leaving a hydroxyl group in the active site (*26*). The proton required for this step is also taken up through the D pathway.

The aa_3-type cytochrome *c* oxidase of *Rhodobacter sphaeroides* is highly similar to the catalytic core of the mitochondrial oxidase (*10*, *27*, *28*). The bacterial oxidase is composed of four subunits, where subunits I, II, and III are the same as their counterparts in the mitochondrial enzyme and subunit IV is small peptide with no homology to a mitochondrial subunit (*10*, *29*). Subunit III contains seven transmembrane helices and little in the way of extramembrane loops; it binds to subunit I opposite the two transmembrane helices of subunit II (*10*). Even though subunit III does not contain a redox center, it is clearly a member of the ancestral catalytic core of the mitochondrial oxidase, since it is encoded in the mitochondrial genome (*30*), its primary sequence is highly conserved [45% identity between *R. sphaeroides* and humans (*31*)], and its unique two-domain structure is seen in both the mitochondrial and the *R. sphaeroides* oxidase (*10*, *27*). In the absence of subunit III, the I−II oxidase of *R. sphaeroides* inactivates with turnover, such that its catalytic lifetime is less than 0.5% that of the normal oxidase containing subunit III (*32*). Suicide inactivation involves irreversible alterations at the heme a_3-Cu_B active site that culminate in the complete loss of Cu_B from the enzyme. Thus, one of the key functions of subunit III in the normal oxidase is to protect the integrity of the Cu_B center during catalytic turnover. The rate of suicide inactivation increases dramatically with increasing pH (*32*). During studies of the inactivating oxidase it became obvious that the initial rate of O_2 reduction by the I−II oxidase, prior to the onset of suicide inactivation, was also considerably more affected by the bulk pH than was the normal oxidase that contained subunit III. This pH dependence of the initial rate was completely reversible and suggested that the proton uptake characteristics of the I−II oxidase may be substantially different from those of the normal enzyme.

Here, we have examined the rate of proton uptake through the D pathway during the reduction of O_2 by fully reduced I−II oxidase of *R. sphaeroides*. The results indicate that the transfer of protons from bulk water through D132 to E286 is very slow at physiologic pH (*7*−*9*) in the absence of subunit III but as rapid as the normal oxidase at low pH values. We propose that another important role for subunit III is to maintain rapid proton uptake by the D pathway in the physiologic pH range.

MATERIALS AND METHODS

Enzyme Purification. ΔCoxIII, the aa_3-type oxidase that assembles in the absence of subunit III in *R. sphaeroides*, was isolated using histidine affinity chromatography as described in Bratton et al. (*32*). For most of the experiments presented here ΔCoxIII was further purified by high-resolution anion-exchange chromatography using a 2 mL DEAE-5PW column (TosoHaas) or a 6 mL Resource Q column (Pharmacia) on an FPLC[1] system, essentially as in Bratton et al. (*33*), to remove subunit I*a*, a free form of subunit I that contains a single heme A. For some experiments ΔCoxIII was used without this further purification, since it was determined that the presence of the catalytically inactive subunit I*a* had no effect on the experiments. For clarity, the term "I−II oxidase" is used throughout to describe the oxidase lacking subunit III. After purification, the I−II oxidase was exchanged into 0.1 M Hepes (pH 7.4) and 0.2% *n*-dodecyl β-D-maltoside (LM) on a PD-10 column (Pharmacia), rapidly frozen in liquid nitrogen, and stored at −80 °C until use.

CO Binding and Flow-Flash Experiments. The enzyme, typically diluted to 15 μM in the appropriate buffer solution (see figure legends), was transferred to an anaerobic cuvette, and the electron mediator phenazine methosulfate (PMS) was added to 0.7 μM. Nitrogen was exchanged for air using a vacuum apparatus, the enzyme was reduced by adding 2 mM ascorbate, and the carbon monoxide adduct was formed by exchanging CO for nitrogen. When necessary, the mixed-valence enzyme ($a^{3+}a_3^{2+}-CO$) was prepared by diluting the enzyme into 0.1 M Tris−KOH, pH 8.5, and 0.1% LM and then incubating enzyme with CO (*34*).

The experimental setup for the flow-flash experiments has been described in detail (*34*). Measurements of absorbance changes associated with reaction of the fully reduced enzyme with oxygen were performed as previously described (*6*, *26*) at three different wavelengths (445, 580, and 830 nm). In experiments in which the pH dependence of the enzyme kinetics was investigated, the enzyme solution was transferred into 100 mM KCl and 0.1% LM using a PD-10 column. It was then mixed in the stopped-flow apparatus with an oxygen-saturated buffer containing 100 mM Caps, 100 mM Bis-Tris propane, 100 mM Mes, adjusted to the desired pH, 0.1% LM, and 1 mM O_2, all at a temperature of 22 °C. Using the wild-type oxidase, this procedure yields results identical to those obtained by prior incubation of the enzyme at the appropriate pH (*13*).

Proton Uptake Measurements. The kinetics of proton uptake during O_2 reduction were measured at pH 8.0 and 5.5 as described previously (*6*, *26*). Briefly, the enzyme was exchanged into an oxygen-saturated buffer-free solution containing 100 mM KCl and 0.1% LM at pH 8.0 or 5.5 using a PD-10 column. At pH 8.0 the pH-sensitive dye phenol red was added to a final concentration of 50 μM whereas at pH 5.5 the pH-sensitive dye bromocresol purple was added to a concentration of 100 μM. Ten to fifteen traces were collected and averaged at 22 °C using the buffer-free solution. To obtain absorbance changes associated only with changes in the proton concentration, a further 10−15 traces were collected and averaged using an oxygen-saturated solution containing 0.1 M Hepes−KOH, pH 8.0, 0.1% LM, and 50 μM phenol red, and these signals were subtracted from those obtained with the buffer-free solution. The same procedure

[1] Abbreviations: FPLC, fast-pressure liquid chromatography; TMPD, *N*,*N*,*N*′,*N*′-tetramethyl-*p*-phenylenediamine; Hepes, 4-(2-hydroxyethyl)-piperazine-1-ethanesulfonic acid; Taps, *N*-[tris(hydroxymethyl)methyl]-3-aminopropanesulfonic acid; Bis-Tris, [bis(2-hydroxyethyl)amino]tris-(hydroxymethyl)methane; Caps, 3-(cyclohexylamino)-1-propanesulfonic acid; Mes, 2-morpholinoethanesulfonic acid; PMS, phenazine methosulfate; LM, *n*-dodecyl β-D-maltoside; CI, confidence interval; TN, turnover number (in e^- s^{-1} aa_3^{-1}); SD, standard deviation.

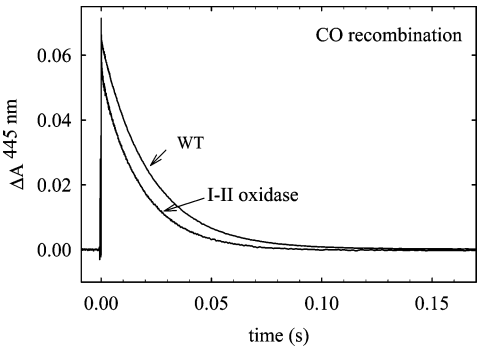

FIGURE 1: Absorbance changes at 445 nm associated with CO dissociation and recombination to the fully reduced wild-type and I−II oxidases. Conditions: 10 μM enzyme, 100 mM Tris-HCl, pH 8.5, 0.1% dodecyl maltoside, and 1 mM CO; $T = 21$ °C. The enzyme was reduced using sodium dithionite. The traces have been normalized to 1 μM reacting enzyme. The absorbance decreases shown by the oxidases were each fit to the sum of two exponentials (see Materials and Methods). This yielded rate constants of 46 s^{-1} (95% of the signal) and 4700 s^{-1} (5%) for the wild-type oxidase and 56 s^{-1} (80%) and 4000 s^{-1} (20%) for the I−II oxidase. Lines showing the fits are completely obscured by the data.

was followed for proton uptake measurements at pH 5.5 except that the buffered solution contained 0.1 M Mes (pH 5.5), 0.1% LM, and 100 μM bromocresol purple.

Fitting. Rate constants of O_2 reduction and proton uptake reactions described in the text were extracted from the absorbance data by nonlinear regression analysis using MatLab 5.3 (The Mathworks, Inc.). The equations and processes used are described in Namslauer et al. (*13*) and Ädelroth et al. (*26*). The standard error of each rate constant was less than 5%, and the residuals of the fits are all less than 10% of the amplitude of the signals.

Steady-State Oxidase Activity Measurements. The rates of steady-state O_2 reduction were measured at various pH values using an oxygen electrode as described in Hosler et al. (*35*) in a reaction mixture of 25 mM Hepes−KOH, 25 mM Taps, 87.5 mM KCl, 0.5 mM EDTA, 0.6 mM TMPD, 3 mM ascorbate, 1 mg/mL phosphatidylcholine (soybean phospholipids), 0.1% LM, and 2−4 pmol of oxidase at 25 °C. Each reaction was initiated by the addition of 40 μM horse heart cytochrome *c*. The rates of nonenzymatic reduction of O_2 by ascorbate/TMPD at each pH were subtracted.

RESULTS

CO Recombination. Figure 1 shows absorbance changes at 445 nm after flash photolysis of CO from the complete four-subunit aa_3-type cytochrome *c* oxidase and the I−II oxidase of *R. sphaeroides*. The initial increase in absorbance is due to dissociation of the CO ligand from heme a_3, while the slower decrease in absorbance reflects the rebinding of CO in the heme a_3−Cu_B active site. The rate of CO recombination in the I−II oxidase was 56 s^{-1}, slightly faster than the rate of 46 s^{-1} observed for the oxidase containing all four subunits. The I−II oxidase also showed more of a rapid component of CO recombination with a rate constant of ~4000 s^{-1} (Figure 1). This component may arise from a fraction of the I−II oxidase which has undergone suicide inactivation prior to isolation of the oxidase from the cell. Suicide inactivation results in the loss of Cu_B (*32*), and several oxidase mutants that have lost Cu_B show rapid recombination of CO (*36*). The presence of small amounts of inactivated oxidase has negligible effects on the experiments presented below since the inactivated oxidase cannot form the oxyferryl intermediates **P** and **F** (*32*), and it shows extremely slow rates of internal electron transfer (Millett and Hosler, unpublished results).

Interheme Electron Transfer. The intrinsic (true) rate of electron transfer between hemes *a* and a_3 can be measured from heme absorbance changes that follow flash photolysis of CO from oxidase in which the heme a_3−Cu_B center is reduced while heme *a* and Cu_A are oxidized (*37*). Flash-induced dissociation of CO from heme a_3 lowers its apparent redox potential, which provides the driving force for reverse electron transfer from heme a_3 to heme *a*. Using the normal *R. sphaeroides* oxidase the rate constant of this electron transfer has previously been measured to be 4.4×10^5 s^{-1} ($\tau = 2$ μs) (*38*). Figure 2A shows absorbance changes at 445 nm after flash-induced dissociation of CO from the mixed-valence I−II oxidase and the normal (WT) oxidase. The initial increase in absorbance is associated with the dissociation of CO from heme a_3. The following decrease in absorbance, associated with the oxidation of heme a_3 and the reduction of heme *a*, displayed rate constants of 4.1×10^5 s^{-1} and 4.4×10^5 s^{-1} for the wild-type and I−II oxidases, respectively. A kinetic difference spectrum of interheme electron transfer by the I−II oxidase was created by fitting the kinetic transients collected at wavelengths between 420 and 460 nm to an exponential function and then plotting the extrapolated amplitude of the absorbance decrease as a function of wavelength (i.e., the absorbance difference of the 2 μs kinetic phase at $t \rightarrow \infty$ and at $t = 0$). The kinetic difference spectrum for the I−II oxidase (Figure 2B) is compared to that of the four-subunit enzyme, which was previously determined to show electron transfer from heme a_3 to heme *a* in 80% of the enzyme population. The comparison shows that the extent of interheme electron transfer was the same for the wild-type oxidase and the I−II oxidase.

At pH values greater than 8, the 2 μs electron-transfer step is followed by a slower heme absorbance change that is associated with the release of a proton from the active site through the K pathway and not the D pathway (*2*, *34*). The kinetics of this reaction were measured at 598 nm (Figure 2C) in order to avoid overlapping signals from the recombination of CO with heme a_3 (*2*, *34*). Rate constants of 410 s^{-1} and 340 s^{-1} were measured for the wild-type and I−II oxidases, respectively (Figure 2C), suggesting that the absence of subunit III does not significantly alter the proton-transfer properties of the K pathway.

Electron Transfer during the Reaction of the Fully Reduced Enzyme with O_2. The reactions of both the fully reduced normal oxidase and I−II oxidase with dioxygen were monitored as time-resolved absorbance changes at 445 and 580 nm (Figure 3). Different phases of this reaction reveal the rates of formation of various intermediates in the reduction of O_2 to water (*26*). At 445 nm the *increase* in absorbance at $t = 0$ is due to flash-induced dissociation of CO from reduced heme a_3. For the normal oxidase at pH 8.0, the following decrease in absorbance at 445 nm (Figure 3A) is associated with O_2 binding to reduced heme a_3 ($k = 1.4 \times 10^5$ s^{-1}), followed by the oxidation of hemes *a* and a_3 and formation of the "peroxy" intermediate, $\mathbf{P_R}$ ($k = 2.5 \times 10^4$ s^{-1}). The $\mathbf{P_R}$ intermediate appears to be an oxyferryl form

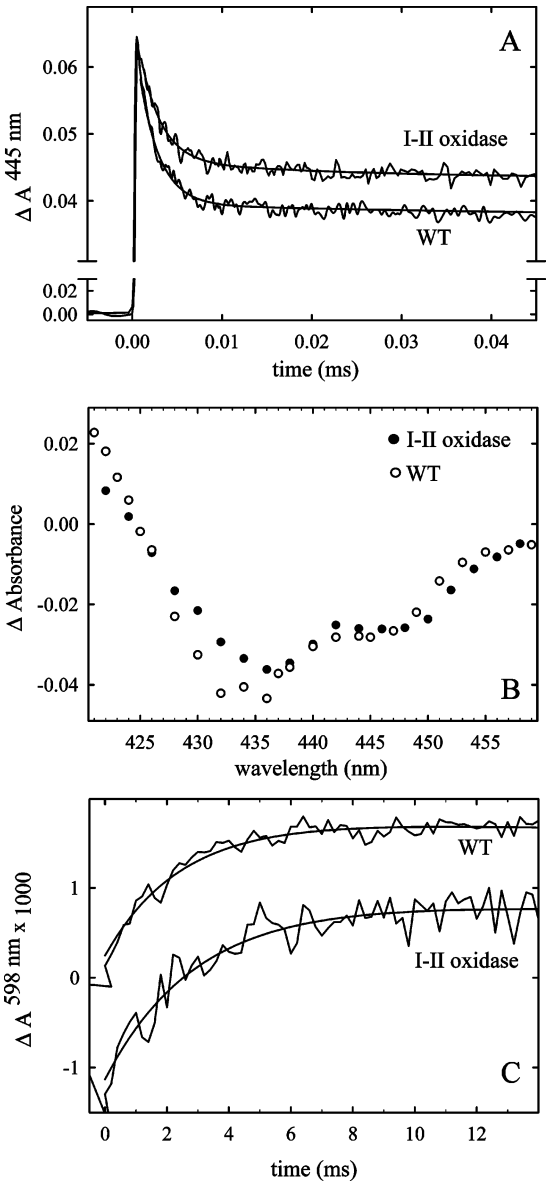

FIGURE 2: Electron transfer from heme a_3 to heme *a* after flash photolysis of CO from the mixed-valence wild-type and I−II oxidases. (A) Absorbance changes at 445 nm due to reverse electron transfer. Experimental conditions were the same as those in Figure 1, except that sodium dithionite was not added. The traces have been scaled to 1 μM reacting enzyme. The absorbance decreases following the initial rapid absorbance increase (see text) were both fit to the sum of two exponentials (shown as smooth lines through the data), one representing rapid electron transfer from heme a_3 to heme *a* and a minor component due to further electron transfer between heme *a* and Cu_A (*59*). For the wild-type oxidase, 90% of the absorbance decrease exhibits a rate of 4.1×10^5 s^{-1} ($a_3 \rightarrow a$) and 10% has a rate of 4.4×10^4 s^{-1} ($a \rightarrow Cu_A$). For the I−II oxidase 80% of the absorbance decrease has a rate of 4.4×10^5 s^{-1} ($a_3 \rightarrow a$) while 20% has a rate of 3.0×10^4 s^{-1} ($a \rightarrow Cu_A$). (B) Kinetic difference spectra of the 2 μs phase (electron transfer from heme a_3 to heme *a*) for the wild-type and I−II oxidases. See text for details. (C) Absorbance changes at 598 nm associated with a millisecond phase of proton release from the active site following flash photolysis of CO from the mixed-valence wild-type and I−II oxidases. Heme *a* absorbance is monitored at 598 nm since this is an isosbestic point for the optical changes resulting from CO recombination (*2*, *34*). The proton release associated with this absorbance change occurs in the K pathway (*2*, *34*). The absorbance traces of the two oxidases are offset for clarity. The lines through the data are fits to single-exponential functions yielding rates of 410 s^{-1} for the wild-type oxidase and 340 s^{-1} for the I−II oxidase.

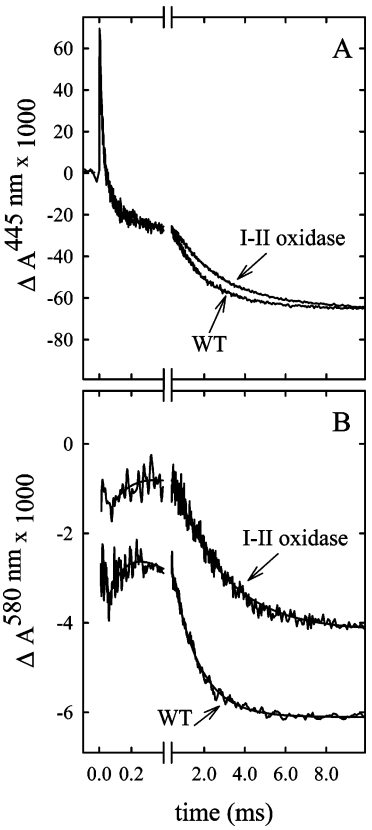

FIGURE 3: Absorbance changes at 445 nm (A) and 580 nm (B) associated with the reaction of fully reduced wild-type or I−II oxidase with O_2, initiated by flash photolysis of CO. An absorbance decrease at 580 nm at $t = 0$ due to a laser artifact has been truncated for clarity. After mixing the solution contained 100 mM Hepes−KOH, pH 8.0, 0.1% dodecyl maltoside, 1−2 μM reacting enzyme, and 1 mM O_2; $T = 22$ °C. The traces have been scaled to 1 μM reacting enzyme. The initial absorbance decrease at 445 nm in panel A, up to 400 μs, was fit to a sum of three exponentials yielding rate constants of 1.4×10^5 s^{-1}, 2.5×10^4 s^{-1}, and 8000 s^{-1}. The first rate is associated with the binding of O_2 to the enzyme, the second with the formation of $\mathbf{P_R}$, and the third with the $\mathbf{P_R} \rightarrow \mathbf{F}$ transition (*26*). The absorbance decrease from 0.4 to 10 ms is due to the final $\mathbf{F} \rightarrow \mathbf{O}$ transition, and the data in this region were fit by locking the three rates given above and fitting a fourth exponential. This yielded rates for the $\mathbf{F} \rightarrow \mathbf{O}$ transition of 800 s^{-1} for the wild-type oxidase and 400 s^{-1} for the I−II oxidase. None of the fits of the 445 nm absorbance traces are shown since they are completely obscured by the data. At 580 nm (panel B) only the formation of $\mathbf{F}$ ($\mathbf{P_R} \rightarrow \mathbf{F}$) and the disappearance of $\mathbf{F}$ ($\mathbf{F} \rightarrow \mathbf{O}$) are seen as absorbance increases and decreases, respectively. Each data set was fit to the sum of two exponentials yielding rates for the $\mathbf{P_R} \rightarrow \mathbf{F}$ transition of 8000 s^{-1} for the wild-type oxidase and 6000 s^{-1} for the I−II oxidase, and rates for the $\mathbf{F} \rightarrow \mathbf{O}$ transition of 770 s^{-1} for the wild-type oxidase and 400 s^{-1} for the I−II oxidase. The fits are shown as smooth lines through the data.

of heme a_3 (a_3^{4+}=O) plus a hydroxyl group on Cu_B (Cu_B−OH^-) (*16*, *18*, *23*, *24*). The ferryl intermediate (**F**) is then formed with a rate constant of 8000 s^{-1} by protonation of the hydroxyl group on Cu_B (*26*). The same rate for the $\mathbf{P_R} \rightarrow \mathbf{F}$ transition is measured from the *increase* in absorbance at 580 nm (Figure 3B) since the **F** intermediate shows an absorbance maximum at 580 nm (*39*). Finally, a slow decrease in absorbance at both wavelengths, with a rate constant of ~800 s^{-1} in the wild-type enzyme, shows formation of the fully oxidized enzyme (the $\mathbf{F} \rightarrow \mathbf{O}$ transition). All of the kinetic phases seen with the normal four-subunit oxidase at pH 8 were also seen with the I−II

oxidase (Figure 3), consistent with normal oxygen reduction chemistry. Up to the formation of **F** the transition rates of the I−II oxidase were the same as those of the normal oxidase. However, the conversion of **F** to **O** by the I−II oxidase was 2-fold slower than the normal oxidase at pH 8 (Figure 3).

The rate of the **F** → **O** transition increased as the pH of the bulk solvent decreased (Figure 4A). Comparison of the pH dependence of the **F** → **O** transition rate of the I−II oxidase to that of the normal oxidase (Figure 4B) reveals two differences. First, the pH dependence profile of the I−II oxidase is shifted to more acid values, with an apparent pK_a of 6.8, considerably lower than the apparent pK_a of 8.6 measured with the normal enzyme. Second, the maximum rate of the **F** → **O** transition at low pH was approximately 2-fold *faster* with the I−II oxidase (∼1600 s^{-1}) than with the four subunit enzyme (∼900 s^{-1}).

In contrast, the slope of the absorbance increase at 580 nm, associated with the $\mathbf{P_R} \rightarrow \mathbf{F}$ transition of the I−II oxidase, showed little difference between pH 5.5 and pH 10 (Figure 4A). The time constant of the $\mathbf{P_R} \rightarrow \mathbf{F}$ transition over this pH range was 130 ± 60 μs (SD, $n = 6$), similar to the rate measured with the wild-type enzyme at pH 9 and below ($\tau \cong 120$ μs) (*13*, *40*). However, while the rate and extent of the $\mathbf{P_R} \rightarrow \mathbf{F}$ transition in the wild-type oxidase decline above pH 9.0 (*13*, *40*), the I−II oxidase still formed intermediate **F** at a rapid rate at pH 10 (Figure 4A).

Proton Uptake during the Reaction of the Fully Reduced Enzyme with O_2. The rate of proton uptake during the reaction of the fully reduced oxidase with oxygen was measured by following the absorbance changes of pH-sensitive dyes in the absence of exogenous buffer. With the normal *R. sphaeroides* oxidase the $\mathbf{P_R} \rightarrow \mathbf{F}$ and the **F** → **O** transitions are each associated with the uptake of approximately one proton through the D pathway with rate constants of 10600 s^{-1} and 600 s^{-1}, respectively, at pH 8 (Figure 5). For the I−II oxidase, the faster of the two phases was not observed in an otherwise identical experiment (Figure 5). Rather, a single slow phase of proton uptake predominated, with a rate constant of 350 s^{-1}. The amplitude of the slow phase was approximately the sum of the two phases measured with the normal four-subunit oxidase, indicating a slow uptake of approximately two protons. Thus, at pH 8 the I−II oxidase showed no rapid proton uptake during the $\mathbf{P_R} \rightarrow \mathbf{F}$ transition; only slow proton uptake was observed over the time scale of both the $\mathbf{P_R} \rightarrow \mathbf{F}$ and **F** → **O** transitions. The rate of proton uptake through the D pathway of the I−II oxidase is pH dependent, however, since at pH 5.5 rapid proton uptake during the time scale of the $\mathbf{P_R} \rightarrow \mathbf{F}$ transition was restored (Figure 5B). Kinetic analysis of the proton uptake tracing at pH 5.5 (Figure 5B) revealed the presence of a rapid phase of proton uptake with a rate constant of 7900 s^{-1}, similar to that of the wild-type oxidase at pH 8.0, and a slower phase of 1600 s^{-1} that matches the rate of the **F** → **O** transition by the I−II oxidase at low pH (Figure 4B).

The recovery of rapid proton uptake by the I−II oxidase at pH 5.5 was also evidenced by the presence of a rapid phase of Cu_A oxidation at this pH (Figure 6). Electron transfer from Cu_A to heme *a* only occurs during the $\mathbf{P_R} \rightarrow \mathbf{F}$ transition if Glu 286 is rapidly reprotonated via the D pathway, since the anionic form of Glu 286 slows electron transfer to heme *a* due to an electrostatic interaction between the carboxylate anion and the heme (*41*). The initial very fast absorbance increase at 830 nm (Figure 6) is due to the photolysis of CO from heme a_3. The rate of Cu_A oxidation at pH 5.5, beginning at $t = 50$ μs, indicates rapid electron transfer (10890 s^{-1}) from Cu_A to heme *a* during the $\mathbf{P_R} \rightarrow \mathbf{F}$

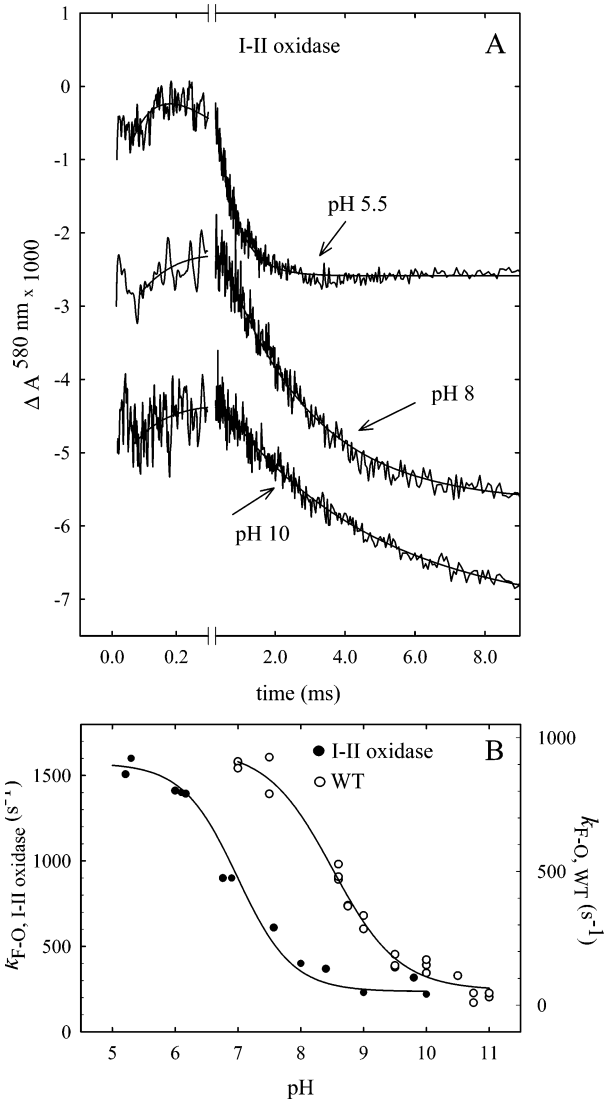

FIGURE 4: pH dependence of the $\mathbf{P_R} \rightarrow \mathbf{F}$ and **F** → **O** transitions of the I−II oxidase. (A) Absorbance changes at 580 nm following flash photolysis of CO from the fully reduced I−II oxidase at pH 5.5, 8, and 10. An absorbance decrease at $t = 0$, due to a laser artifact, has been truncated for clarity. After mixing, the solution contained 100 mM CAPS, 100 mM Bis-Tris propane, 100 mM Mes, adjusted to the indicated pH, 0.1% dodecyl maltoside, and 1 mM O_2; $T = 22$ °C. Fits to the data (smooth lines) were prepared as described in Figure 3. The rates derived for the $\mathbf{P_R} \rightarrow \mathbf{F}$ transition were 8500 s^{-1} at pH 5.5, 6000 s^{-1} at pH 8.0, and 7200 s^{-1} at pH 10.0, while the rates derived for the **F** → **O** transition were 1600 s^{-1} at pH 5.5, 400 s^{-1} at pH 8.0, and 220 s^{-1} at pH 10.0. (B) pH dependence of the **F** → **O** transition rate in the wild-type and I−II oxidases. The rates of the **F** → **O** transition were obtained at several different pH values as described above. The solid lines are fits to the sigmoidal function that assumes a single pK_a value using the equation $k_{\mathbf{F}\rightarrow\mathbf{O}} = k_{\mathbf{F}\rightarrow\mathbf{O}\min} + (k_{\mathbf{F}\rightarrow\mathbf{O}\max} - k_{\mathbf{F}\rightarrow\mathbf{O}\min})/(1 + 10^{\mathrm{pH}-\mathrm{p}K_a})$. The fits yield an apparent pK_a for the I−II oxidase of 6.8 [with a 95% confidence interval (CI) of 6.68−7.01] and 8.6 for the wild-type oxidase (with a 95% CI of 8.53−8.68). Note the different scales for the I−II and wild-type enzyme data, respectively, on the ordinate. The data for the wild-type oxidase have been presented previously (*40*).

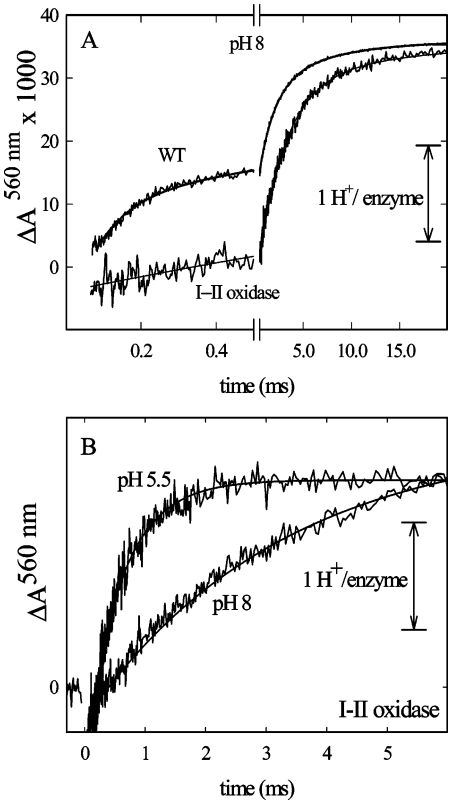

FIGURE 5: Proton uptake by the I−II oxidase is slower than that by the wild-type oxidase at pH 8.0 but rapid at pH 5.5. (A) Absorbance traces at 560 nm associated with changes in the protonation state of the pH dye phenol red are shown. The traces in the figure are the difference between traces obtained at 560 nm with an unbuffered (KCl) solution and a buffered (Hepes) solution, both at pH 8. The traces have been scaled so that the length of the arrow corresponds to 1 H^+/enzyme molecule (see Materials and Methods for details). The trace for the wild-type oxidase was fit to a sum of three exponentials (smooth line): 40% with a rate of 10600 s^{-1} (similar to the rate of the $\mathbf{P_R} \rightarrow \mathbf{F}$ transition, Figure 3B), 40% with a rate of 600 s^{-1} (similar to the rate of the $\mathbf{F} \rightarrow \mathbf{O}$ transition, Figure 3B), and 20% with a rate of 140 s^{-1}. The event(s) associated with this slower rate of proton uptake remains unidentified. The trace for the I−II oxidase fit best to two exponentials (smooth line): 82% with a rate of 350 s^{-1} (similar to the rate of the $\mathbf{F} \rightarrow \mathbf{O}$ transition of the I−II oxidase, Figures 3B and 4) and 18% with a rate of 61 s^{-1}. Again, the event(s) associated with the slower rate of proton uptake is (are) not known. The gradual increases seen between 0.2 and 0.5 ms in the wild-type trace and between 0 and 0.5 ms in the I−II oxidase trace are the beginning of the slower phases of proton uptake. (B) The experiment at pH 5.5 was performed as described above but using bromocresol purple (Materials and Methods). The pH 8 data are the same as that shown on different time scales in panel A. The scale on the ordinate is not shown because absorbance changes were recorded with two different dyes at different dye concentrations. The traces have been scaled to show proton uptake per reacting enzyme. Initial absorbance changes due to a laser artifact at $t = 0$ have been truncated. The data at pH 8.0 are fit as described above to a predominant rate of 350 s^{-1}. The trace obtained at pH 5.5 was fit to the sum of two exponentials (smooth line): 55% with a rate of 7900 s^{-1} and 45% with a rate of 1600 s^{-1}.

transition and slower electron transfer (1330 s^{-1}) during the $\mathbf{F} \rightarrow \mathbf{O}$ transition (Figure 6). This indicates the presence of rapid proton transfer from D132 to E286 in the I−II oxidase at pH 5.5 during the $\mathbf{P_R} \rightarrow \mathbf{F}$ transition, similar to that seen in the normal oxidase containing subunit III at pH 8.0. The slow rate of Cu_A oxidation beginning at $t = 50$ μs at pH 8.0 (Figure 6) confirms that rapid proton uptake does *not* take place during the time scale of the $\mathbf{P_R} \rightarrow \mathbf{F}$ transition in the

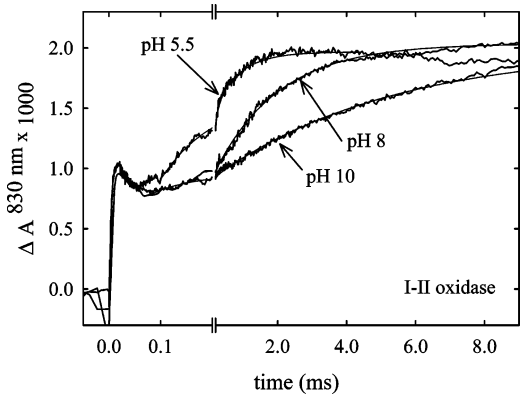

FIGURE 6: Electron transfer from Cu_A to heme *a* following the photolysis of CO from fully reduced I−II oxidase at pH 5.5, 8, and 10. Experimental conditions were as in Figure 4. The initial absorbance increase is due to CO photolysis from heme a_3 and the rapid binding of O_2. Fits to the data begin at $t = 50$ μs, after these events, in the region where the increase in absorbance at 830 nm corresponds to the oxidation of Cu_A as it transfers an electron to heme *a* (*41*). At pH 5.5, the oxidation of Cu_A fits well to a sum of two exponentials, with 74% of the signal corresponding to a rate of 10890 s^{-1} and 26% of the signal corresponding to rate of 1330 s^{-1}. At pH 8.0 and 10, the data are fit to single exponentials yielding rates of 525 s^{-1} and 193 s^{-1}, respectively.

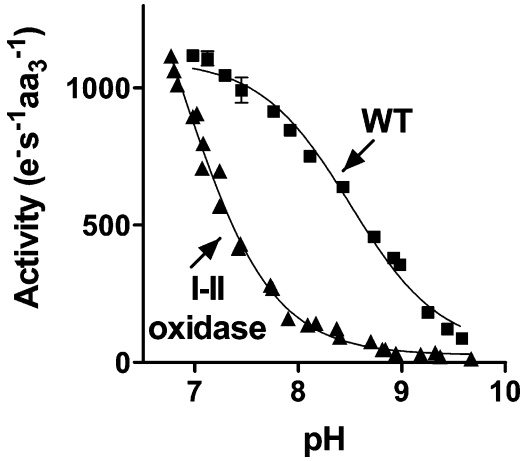

FIGURE 7: The pH dependence of steady-state O_2 reduction by the I−II oxidase is shifted to more acid values. The initial rate of steady-state O_2 reduction was determined at different pH values as described in Materials and Methods. The lines through each data set are nonlinear regression curves (GraphPad Prism 3.0, GraphPad Software) generated by a sigmoidal function that assumes a single pK_a value using the equation $TN = TN_{min} + (TN_{max} - TN_{min})/(1 + 10^{pH-pK_a})$. The fits yield a p$K_a$ of 7.2 for the I−II oxidase (95% CI from 7.19 to 7.33) and 8.5 for the wild-type oxidase (95% CI from 8.39 to 8.60).

I−II oxidase at pH 8.0, in contrast to the wild-type oxidase (*41*).

pH Dependence of Steady-State Oxidase Turnover. The rate of steady-state O_2 reduction by cytochrome *c* oxidase is dependent upon the bulk pH in that the rate declines with increasing pH (*42*−*44*). Previous analyses of the pH dependence of detergent-solubilized and reconstituted cytochrome oxidase show that the activity measured between pH 5 and pH 8.5 can yield up to three apparent pK_a values (*42*, *43*). Thus, it is likely that steady-state oxidase activity is controlled by the protonation state of one or more groups involved in the transfer of protons to the active site. The pH dependence of the initial rate of O_2 reduction by the I−II oxidase of *R. sphaeroides* is markedly different from that of

Scheme 1: Proton Uptake during the Single-Turnover Reduction of O_2 by Fully Reduced Wild-Type and I−II Oxidase at pH 8.0[a]

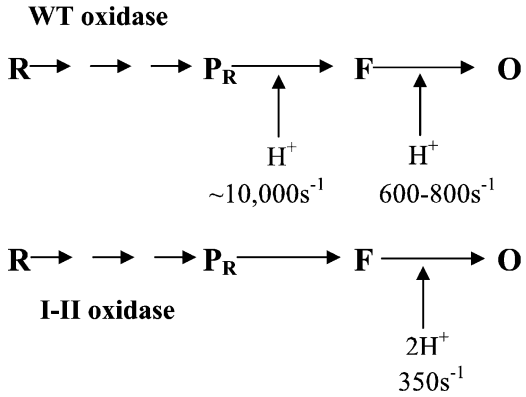

[a] **R** = fully reduced oxidase.

the normal enzyme that contains subunit III in that the activity of the I−II oxidase declines sharply between pH 7 and pH 8 (Figure 7). By fitting the oxidase activity profiles between pH 7 and pH 10 to a single pK_a value (Figure 7), apparent pK_a values for steady-state O_2 reduction of 8.5 and 7.2 were obtained for the normal oxidase and the I−II oxidase, respectively. Only rates between pH 7 and pH 10 were analyzed by the curve fits, although extending the data to pH 6.5 did not alter the apparent pK_a values. Below pH 6.5 the ability of cytochrome *c* to bind to the oxidase begins to limit activity (*43*). The rates shown here were measured using a high cytochrome *c* concentration (40 μM). Plots of V_{max} vs pH (not shown) yield the same result as Figure 7.

DISCUSSION

The rate of CO binding to the active site of the I−II oxidase is similar to the wild-type oxidase, and the intrinsic rate of electron transfer between hemes a_3 and *a* is the same for the two oxidase forms. These findings are consistent with previous spectroscopic and functional studies that show that the environments of the redox centers of cytochrome oxidase are not significantly altered by the absence of subunit III (*32*, *33*, *45*). However, the results presented here show that the removal of subunit III alters the apparent pK_a of the D pathway in subunit I such that proton uptake at physiologic pH (*7*−*8*) is greatly slowed.

Subunit III Affects the Rate of Proton Transfer from Bulk Water to D132 to E286 in the D Pathway of Subunit I. During the single-turnover reduction of O_2 by fully reduced cytochrome *c* oxidase, one proton is taken up during the **P$_R$** → **F** transition and another during the conversion of **F** to **O** (Scheme 1); both of these protons move through the D pathway to the heme a_3−Cu_B active site (*8*). The removal of subunit III from cytochrome *c* oxidase eliminates rapid proton uptake during the **P$_R$** → **F** transition and slows proton uptake through the D pathway approximately 30-fold at pH 8.0 (Scheme 1).

A simplified model of the D pathway (Scheme 2) includes three protonatable groups, D132, E286, and the O_2 reduction intermediates **P$_R$** and **F**. These groups anchor two hydrogen-bonded series of waters that perform rapid proton transfer. Since the pK_a of the **P$_R$** and **F** intermediates is very high, proton transfer from E286 to the active site may be considered irreversible. One key question is whether the

Scheme 2: Simplified Model of the D Pathway in Subunit I

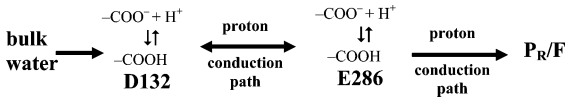

removal of subunit III primarily inhibits proton transfer from D132 to E286 or from E286 to the active site or both.

During the **P$_R$** → **F** transition no electrons are transferred, but a proton is abstracted from E286 and transferred to the hydroxyl group on Cu_B (*12*, *25*). In the normal oxidase, the **P$_R$** → **F** transition reaches a maximum rate around 10000 s^{-1} at pH 8 and below, where E286 is fully protonated at the beginning of the reaction (and **P$_R$**, of course, is fully deprotonated) (*13*, *40*). Thus, the normal rate of proton transfer from E286 to the active site is approximately 10000 s^{-1}. Subsequently, E286 is rapidly and stoichiometrically reprotonated via D132 at a rate modeled to be greater than 10000 s^{-1} (*12*, *13*).

In the I−II oxidase, the **P$_R$** → **F** transition occurs at the normal rate; thus the rate of proton transfer from E286 to the active site must be normal: ~10000 s^{-1}. However, the rapid uptake (>10000 s^{-1}) of one proton that normally accompanies the **P$_R$** → **F** transition is lacking. Only the beginning of a very slow uptake of two protons is observed on the time scale of this transition. Since the rate of proton transfer from E286 to the active site is normal, the absence of rapid proton uptake in the I−II oxidase must be due to some alteration in the path from bulk water to E286, including the initial protonation of D132. At low pH (5.5−6.0) rapid proton uptake into the D pathway is fully restored to the I−II oxidase. The reversible nature of D pathway function by pH suggests the alteration of the pK_a of a rate-controlling group in the absence of subunit III as opposed to more global structural instability due to absence of the subunit.

During the conversion of **F** to **O**, the final step in the single-turnover reaction, an electron is transferred from heme *a* to heme a_3, and a second proton is abstracted from E286 and transferred to the active site (*26*). While the **F** → **O** transition is slow in the normal oxidase, it is even slower in the I−II oxidase. The rate of this transition at pH 8.0 (400 s^{-1}) closely matches the rate of proton uptake (350 s^{-1}), strongly suggesting that the **F** → **O** transition of the I−II oxidase is limited by the rate of proton delivery to E286 via D132. Thus, the apparent pK_a of 6.8 measured for the **F** → **O** transition should also be the apparent pK_a of the D pathway of the I−II oxidase.

Interestingly, at low pH values, where rapid proton uptake through the D pathway is reestablished, the **F** → **O** transition of the I−II oxidase occurs at nearly twice the rate of the normal oxidase. The reason for this is unclear; it could be due to a slight decrease in the redox potential of heme *a*.

Even though the results indicate that the loss of rapid proton transfer above pH 6.8 in the I−II oxidase is due to changes around D132 in the D pathway, the environment of E286 may also be altered. In the wild-type oxidase, the rate of the **P$_R$** → **F** transition declines at pH values above 9, yielding an apparent pK_a of 9.4 for E286 (*13*). In the I−II oxidase, however, the **P$_R$** → **F** transition remains rapid and complete up to pH 10. Thus, E286 of the I−II oxidase appears to be fully protonated at pH 10 prior to electron flow,

indicating an increase in its pK_a as compared to the wild-type enzyme. Indeed, recent experiments indicate that the removal of subunit III can alter the environment of E286 (*46*).

Structural Explanations for Alteration of the D Pathway in the Absence of Subunit III. The analysis presented above indicates that the removal of subunit III slows proton transfer from bulk water through D132 to E286 but not from E286 to the active site (Scheme 2). Two possible explanations for this can be supported, in part, by examination of the recent high-resolution structure of the aa_3-type oxidase of *R. sphaeroides* (*10*). One, the pK_a of D132 may be lower in the absence of subunit III, thus slowing proton entry. Two, the effectiveness of a proton antenna that delivers protons to D132 may be diminished by the removal of subunit III.

The effect of removing subunit III is remarkably similar to the effect of adding micromolar amounts of Zn^{2+} to the wild-type oxidase that contains subunit III (*47*). In both cases rapid proton uptake during the $\mathbf{P_R} \rightarrow \mathbf{F}$ transition is lost and replaced by the slower uptake of two protons on the millisecond time scale. In addition, either the addition of zinc or the removal of subunit III slows the rate of the $\mathbf{F} \rightarrow \mathbf{O}$ transition to the same extent.

Zinc appears to bind near the mouth of the D pathway (*47*) [zinc also binds on the outside of the enzyme in the presence of a transmembrane voltage gradient (*48*)]. Recent results (*46*) indicate that neither subunit III nor D132 is necessary for zinc binding at its site near the D pathway entrance. If D132 does not bind zinc, but Zn^{2+} binds near D132, the cationic metal is likely to lower the pK_a of the carboxylate residue by stabilizing the deprotonated form through an electrostatic interaction. Since removing subunit III has the same effect on proton uptake as adding zinc, it is reasonable to propose that at least one of the effects of removing subunit III is to lower the pK_a of D132, thus lowering the efficiency of proton uptake at physiologic pH.

The crystal structure of the normal *R. sphaeroides* oxidase (*10*) shows that D132 is not completely surface exposed. Rather, it is situated at the bottom of a shallow depression formed by a ring of residues at an interface of subunits I and III (Figure 8). One arc of this ring is composed of hydrophobic residues of subunit III (Figure 8). In the absence of subunit III, the carboxylate of D132 will be more exposed to bulk water. Thus, it seems likely that the pK_a of D132 will decline in the absence of subunit III. Since the effective rate of proton transfer from D132 to E286 will be directly proportional to the fraction of D132 that is protonated, a decline in its pK_a will lower the rate of proton uptake at pH values above the new pK_a. If, for example, the actual rate of proton transfer through D132 to E286 in the normal oxidase is assumed to be 20000 s^{-1} at pH 8, a decline of the pK_a of D132 by a little less than two pH units would lower the proton-transfer rate to the rate observed in the I−II oxidase (~350 s^{-1}).

An alternative or additional explanation for slow proton uptake by the I−II oxidase at pH 8 involves a proton-collecting antenna (*49*) that may assist in the uptake of protons into the D pathway. In theory, such antenna are composed of carboxylate and histidine residues, where the carboxylates attract protons electrostatically and the histidine residues function as a local reservoir of protons (*50*, *51*).

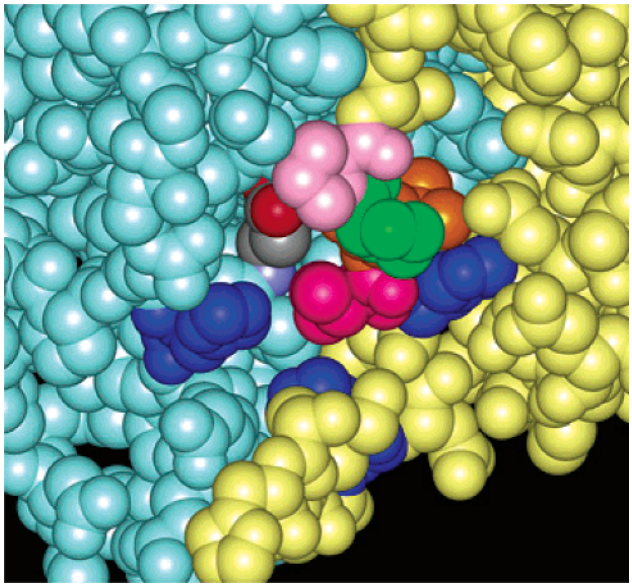

FIGURE 8: A ring of residues from subunits I and III surrounds D132. The image, prepared using WebLab ViewerPro (Molecular Simulations) and the high-resolution structure of wild-type cytochrome *c* oxidase of *R. sphaeroides* (*10*), shows part of the cytoplasmic (matrix) surface of cytochrome oxidase with the atoms depicted in a space-filling format using van der Waals radii. Except for the eight highlighted residues, subunit I is light blue and subunit III is light yellow. D132 is near the center of the image with its atoms colored by elements (N, blue; C, gray; O, red); D132 sits within a shallow depression (5−8 Å in depth) with one of its carboxylate oxygens pointing toward the surface. Four residues of subunit III form part of the ring around D132 (Ile 11, magenta; Leu 12, orange; Pro 13, green; and Pro 14, pink) while three histidines that may form part of the proton antenna for the D pathway are shown in blue. Clockwise, from right to left, these are His 10 and His 7 of subunit III and His 549 of subunit I.

The fastest proton uptake event observed during the reaction of the fully reduced wild-type enzyme and oxygen occurs during the $\mathbf{P_R} \rightarrow \mathbf{F}$ transition (~10000 s^{-1} at pH 8.0). With the wild-type enzyme, about the same rate is observed at pH 9 (*13*). Hence, the proton uptake rate at pH 9 is about a factor of 100 faster than that expected if proton uptake was limited by the rate of proton diffusion, through water, to the entry point of the D pathway ($k_{on} = 4 \times 10^{10}$ M^{-1} s^{-1}; for review see ref *51*). Consequently, it is likely that in cytochrome *c* oxidase there exists a local, protein-derived buffer that assists in proton uptake into the D pathway. The N-terminal tail of subunit III contains three histidine residues at positions 3, 7, and 10; the imidazoles of histidines 7 and 10 are within 9−11 Å of the carboxylate group of D132 (Figure 8). Thus, it is possible that the removal of subunit III eliminates some of the protein-derived buffer near the entry point of the D pathway and this slows proton delivery to D132.

Mechanistic Consequences of Altered D Pathway Activity for Steady-State O_2 Reduction, Proton Pumping, and Suicide Inactivation. The fact that proton uptake by the I−II oxidase is slowed by a factor of 30 at pH 8 provides the explanation for the strong inhibition of steady-state O_2 reduction by the I−II oxidase at pH values greater than 7. In the absence of subunit III, the apparent pK_a values of the $\mathbf{F} \rightarrow \mathbf{O}$ transition and steady-state O_2 reduction are similar (6.8 vs 7.2), which strongly suggests that both processes are limited by the rate of proton uptake through D132. It is less clear what limits

the steady-state activity of the wild-type oxidase; proton uptake via the K pathway is a possibility (*52*−*54*).

The subunit III-depleted oxidase of *R. sphaeroides* does pump protons (*46*) albeit with lower efficiency (a lower H^+/e^-) as has previously been noted for other cytochrome *c* oxidases lacking subunit III (*55*−*57*). The results reported here provide two possible explanations for a lower H^+/e^- in the absence of subunit III. Proton pumping apparently takes place during the **P** → **F** and the **F** → **O** steps of the catalytic cycle (*15*, *16*, *58*). The absence of proton uptake during the **P** → **F** transition in the I−II oxidase would impair the pumping event associated with this reaction. In contrast, the matched kinetics of the **F** → **O** transition and proton uptake may allow the pumping reaction to remain coupled during this step of the catalytic cycle. An alternative explanation is that the higher pK_a of E286 in the I−II oxidase diminishes its capability to drive the protonation of the proton acceptor(s) of the pumping apparatus. Alteration of the pK_a of the terminal carboxylate residue of the D pathway has been proposed as an explanation of the lower pumping stoichiometry of the E286A/I112E mutant of *R. sphaeroides* (*40*).

One important consequence of slow proton uptake by the I−II oxidase at pH values above 6.5−7 is that during steady-state (continuous) O_2 reduction the **P** and **F** intermediates will persist for longer periods during the catalytic cycle. This is likely to be significant for the mechanism of the suicide inactivation reaction that takes place at the active site in the absence of subunit III. The rate of suicide inactivation increases with pH (*32*). Thus, an increased probability of suicide inactivation directly correlates with increased lifetimes of the potentially reactive oxyferryl intermediates **P** and **F**, with the implication that irreversible oxyferryl chemistry is involved in the collapse of the active site in the absence of subunit III.

CONCLUSIONS

The absence of subunit III alters the D pathway such that proton transfer through D132 to E286 is very slow at physiologic pH values (7−8), a pH range where proton transfer in the oxidase that contains subunit III is extremely rapid. Rapid proton uptake is restored to the I−II oxidase at lower pH, as indicated by direct measurements of proton uptake *and* by observing the rate at which Cu_A reduces heme *a* during the $\mathbf{P_R}$ → **F** transition. In the absence of subunit III, slow proton uptake into the D pathway appears to become the rate-limiting step for steady-state O_2 reduction by the soluble enzyme. In a coupled system, such as a respiring bacterial cell, proton uptake into the D channel is already challenged by the presence of a membrane potential. Thus, one role for subunit III may be to maintain the functional pK_a of the D pathway at a high enough value that proton uptake from the bacterial cytoplasm or the mitochondrial matrix, each with a pH ∼7.6 or greater, is favored. The pK_a of E286 appears to be elevated in the absence of subunit III. This alteration does not affect the rate of the proton transfer to the active site, but it may affect the ability of E286 to transfer a proton to the proton pump. In contrast to the D pathway, proton transfer through the K pathway, the other proton pathway leading to the active site from the inner surface of the oxidase, appears unaffected by the absence of subunit III.

ACKNOWLEDGMENT

The authors thank Ms. Zi Tan and Mr. Daniel Smith for excellent technical assistance and Drs. Victor Davidson, Denise Mills, Shelagh Ferguson-Miller, and Pia Ädelroth for valuable insights.

REFERENCES

1. Saraste, M. (1999) *Science 283*, 1488−1493.
2. Ädelroth, P., Gennis, R. B., and Brzezinski, P. (1998) *Biochemistry 37*, 2470−2476.
3. Junemann, S., Meunier, B., Gennis, R. B., and Rich, P. R. (1997) *Biochemistry 36*, 14456−14464.
4. Konstantinov, A. A., Siletsky, S., Mitchell, D., Kaulen, A., and Gennis, R. B. (1997) *Proc. Natl. Acad. Sci. U.S.A. 94*, 9085−9090.
5. Verkhovskaya, M. L., García-Horsman, A., Puustinen, A., Rigaud, J. L., Morgan, J. E., Verkhovsky, M. I., and Wikström, M. (1997) *Proc. Natl. Acad. Sci. U.S.A. 94*, 10128−10131.
6. Ädelroth, P., Ek, M. S., Mitchell, D. M., Gennis, R. B., and Brzezinski, P. (1997) *Biochemistry 36*, 13824−13829.
7. Brzezinski, P., and Ädelroth, P. (1998) *Acta Physiol. Scand., Suppl. 643*, 7−16.
8. Brzezinski, P., and Ädelroth, P. (1998) *J. Bioenerg. Biomembr. 30*, 99−107.
9. Iwata, S., Ostermeier, C., Ludwig, B., and Michel, H. (1995) *Nature 376*, 660−669.
10. Svensson-Ek, M., Abramson, J., Larsson, G., Törnroth, S., Brzezinski, P., and Iwata, S. (2002) *J. Mol. Biol. 321*, 329−339.
11. Riistama, S., Hummer, G., Puustinen, A., Dyer, R. B., Woodruff, W. H., and Wikström, M. (1997) *FEBS Lett. 414*, 275−280.
12. Ädelroth, P., Karpefors, M., Gilderson, G., Tomson, F. L., Gennis, R. B., and Brzezinski, P. (2000) *Biochim. Biophys. Acta 1459*, 533−539.
13. Namslauer, A., Aagaard, A., Katsonouri, A., and Brzezinski, P. (2003) *Biochemistry 42*, 1488−1498.
14. Mills, D. A., and Ferguson-Miller, S. (2002) *Biochim. Biophys. Acta 1555*, 96−100.
15. Wikström, M., and Verkhovsky, M. I. (2002) *Biochim. Biophys. Acta 1555*, 128−132.
16. Michel, H. (1999) *Biochemistry 38*, 15129−15140.
17. Ferguson-Miller, S., and Babcock, G. T. (1996) *Chem. Rev. 96*, 2889−2908.
18. Sucheta, A., Szundi, I., and Einarsdóttir, Ó. (1998) *Biochemistry 37*, 17905−17914.
19. Han, S., Takahashi, S., and Rousseau, D. L. (2000) *J. Biol. Chem. 275*, 1910−1919.
20. Hill, B. C. (1994) *J. Biol. Chem. 269*, 2419−2425.
21. Gibson, Q. H., and Greenwood, C. (1963) *Biochem. J. 86*, 541−554.
22. Proshlyakov, D. A., Pressler, M. A., and Babcock, G. T. (1998) *Proc. Natl. Acad. Sci. U.S.A. 95*, 8020−8025.
23. Morgan, J. E., Verkhovsky, M. I., Palmer, G., and Wikström, M. (2001) *Biochemistry 40*, 6882−6892.
24. Zaslavsky, D., and Gennis, R. B. (2000) *Biochim. Biophys. Acta 1458*, 164−179.
25. Smirnova, I. A., Ädelroth, P., Gennis, R. B., and Brzezinski, P. (1999) *Biochemistry 38*, 6826−6833.
26. Ädelroth, P., Ek, M., and Brzezinski, P. (1998) *Biochim. Biophys. Acta 1367*, 107−117.
27. Yoshikawa, S., Shinzawa-Itoh, K., and Tsukihara, T. (1998) *J. Bioenerg. Biomembr. 30*, 7−14.
28. Tomizaki, T., Yamashita, E., Yamaguchi, H., Aoyama, H., Tsukihara, T., Shinzawa-Itoh, K., Nakashima, R., Yaono, R., and Yoshikawa, S. (1999) *Acta Crystallogr., Sect. D: Biol. Crystallogr. 55*, 31−45.
29. Witt, H., and Ludwig, B. (1997) *J. Biol. Chem. 272*, 5514−5517.
30. Anderson, S., Bankier, A. T., Barrell, B. G., de Bruijn, M. H., Coulson, A. R., Drouin, J., Eperon, I. C., Nierlich, D. P., Roe, B. A., Sanger, F., Schreier, P. H., Smith, A. J., Staden, R., and Young, I. G. (1981) *Nature 290*, 457−465.
31. Cao, J., Hosler, J., Shapleigh, J., Revzin, A., and Ferguson-Miller, S. (1992) *J. Biol. Chem. 267*, 24273−24278.
32. Bratton, M. R., Pressler, M. A., and Hosler, J. P. (1999) *Biochemistry 38*, 16236−16245.
33. Bratton, M. R., Hiser, L., Antholine, W. E., Hoganson, C., and Hosler, J. P. (2000) *Biochemistry 39*, 12989−12995.

34. Branden, M., Sigurdson, H., Namslauer, A., Gennis, R. B., Ädelroth, P., and Brzezinski, P. (2001) *Proc. Natl. Acad. Sci. U.S.A. 98*, 5013−5018.
35. Hosler, J. P., Fetter, J., Tecklenburg, M. M., Espe, M., Lerma, C., and Ferguson-Miller, S. (1992) *J. Biol. Chem. 267*, 24264−24272.
36. Brown, S., Rumbley, J. N., Moody, A. J., Thomas, J. W., Gennis, R. B., and Rich, P. R. (1994) *Biochim. Biophys. Acta 1183*, 521−532.
37. Oliveberg, M., and Malmström, B. G. (1991) *Biochemistry 30*, 7053−7057.
38. Namslauer, A., Brändén, M., and Brzezinski, P. (2002) *Biochemistry 41*, 10369−10374.
39. Rich, P. R., Breton, J., Junemann, S., and Heathcote, P. (2000) *Biochim. Biophys. Acta 1459*, 475−480.
40. Gilderson, G., Aagaard, A., and Brzezinski, P. (2002) *Biophys. Chem. 98*, 105−114.
41. Karpefors, M., Ädelroth, P., Zhen, Y., Ferguson-Miller, S., and Brzezinski, P. (1998) *Proc. Natl. Acad. Sci. U.S.A. 95*, 13606−13611.
42. Wilms, J., van Rijn, J. L., and Van Gelder, B. F. (1980) *Biochim. Biophys. Acta 593*, 17−23.
43. Gregory, L. C., and Ferguson-Miller, S. (1988) *Biochemistry 27*, 6307−6314.
44. Einarsdóttir, Ó., Choc, M. G., Weldon, S., and Caughey, W. S. (1988) *J. Biol. Chem. 263*, 13641−13654.
45. Echabe, I., Haltia, T., Freire, E., Goni, F. M., and Arrondo, J. L. (1995) *Biochemistry 34*, 13565−13569.
46. Mills, D., Tan, Z., Ferguson-Miller, S., and Hosler, J. (2003) *Biochemistry 42*, 7410−7417.
47. Aagaard, A., Namslauer, A., and Brzezinski, P. (2002) *Biochim. Biophys. Acta 1555*, 133−139.
48. Mills, D. A., Schmidt, B., Hiser, C., Westley, E., and Ferguson-Miller, S. (2002) *J. Biol. Chem. 277*, 14894−14901.
49. Marantz, Y., Nachliel, E., Aagaard, A., Brzezinski, P., and Gutman, M. (1998) *Proc. Natl. Acad. Sci. U.S.A. 95*, 8590−8595.
50. Marantz, Y., Einarsdóttir, Ó. O., Nachliel, E., and Gutman, M. (2001) *Biochemistry 40*, 15086−15097.
51. Gutman, M., and Nachliel, E. (1990) *Biochim. Biophys. Acta 1015*, 391−414.
52. Verkhovsky, M. I., Morgan, J. E., and Wikström, M. (1995) *Biochemistry 34*, 7483−7491.
53. Wikström, M., Jasaitis, A., Backgren, C., Puustinen, A., and Verkhovsky, M. I. (2000) *Biochim. Biophys. Acta 1459*, 514−520.
54. Tomson, F. L., Morgan, J., Gu, G., Barquera, B., Vygodina, T. V., and Gennis, R. B. (2003) *Biochemistry 42*, 1711−1717.
55. Prochaska, L. J., and Reynolds, K. A. (1986) *Biochemistry 25*, 781−787.
56. Thompson, D. A., Gregory, L., and Ferguson-Miller, S. (1985) *J. Inorg. Biochem. 23*, 357−364.
57. Solioz, M., Carafoli, E., and Ludwig, B. (1982) *J. Biol. Chem. 257*, 1579−1582.
58. Jasaitis, A., Verkhovsky, M. I., Morgan, J. E., Verkhovskaya, M. L., and Wikström, M. (1999) *Biochemistry 38*, 2697−2706.
59. Brzezinski, P. (1996) *Biochemistry 35*, 5611−5615.

BI0341298